16 (2022) 100201

Contents lists available at ScienceDirect

International Journal of Thermofluids

journal homepage: www.sciencedirect.com/journal/international-journal-of-thermofluids

Variation in cooling performance of a bio-based phase change material by adding graphene nanoplatelets with surfactants

Yahya Sheikh, Mehmet Fatih Orhan *, Muhammed Umair, Elmehaisi Mehaisi, Ahmed Azmeer

Department of Mechanical Engineering, College of Engineering, American University of Sharjah, Sharjah, 26666, UAE

ARTICLE INFO

Keywords:
Bio-based PCMs
Latent heat storage
Graphene nano-platelets
Surfactants

ABSTRACT

In this paper, thermal characteristics of various phase change materials induced with additives and surfactants are studied to enhance cooling properties and chemical stability. In this regard, graphene nanoplatelets at various mass fractions are integrated with surfactant-induced-PureTemp PCM and used as a heat sink for an electric heating source. The surfactants considered in this study are sodium dodecyl sulfate, sodium dodecylbenzene sulfonate, and sodium stearoyl lactylate. The thermal characteristics are measured in terms of indices such as thermal conductivity, thermal capacity, and time of reaching the reference temperature. The results indicate that composite samples are superior in cooling when compared to the plain PureTemp PCM. Also, the highest thermal conductivity and phase change enthalpy are recorded in NanoPCM-SDS at 5% GnPs mass fraction and NanoPCM-SSL at 1% GnPs mass fraction amounting to 1.03 W/m.K and 236.5 J/g, respectively. NanoPCM-SSL displayed the longest delay of 1015 s to reach the reference temperature of 43 °C.

1. Introduction

Cooling systems play a vital role in ensuring the reliability and performance of components within many electronic systems. Consequently, there is a growing interest in the study of techniques for the thermal management of electronic devices. In particular, the materials used within such systems play a vital role when the cooling performance of the thermal management system is considered.

Phase change materials are substances that have the distinct ability to absorb or release a large amount of latent thermal energy at a constant temperature while transition of phase during the charging or discharging process [1]. The high heat of fusion exchanged during the charging or discharging process (heating or cooling) while changing phase is due to the principle of latent heat thermal energy storage [2]. This nature of PCMs makes them suitable candidates for cooling systems where the desired temperature is achieved absorbing a large amount of energy. These two attributes are utilized in cooling and heating systems for buildings and energy storage systems[3–6].

Integration of a PCM in such systems introduces a significant potential of improvement in system efficiency, energy savings, and reduction of emissions and environmental impact. This is possible due to energy conservation opportunities through energy storage and release at appropriate times of energy supplied to or demanded from the system. This is substantiated from the study of Azzous et al. [7] where integration of PCMs into a domestic refrigeration system led to an increase of the system's COP by 15%. Further, in the case of the PCM's application as a heat sink, reduced temperatures and a decrease in system heat gain, were observed when PCMs were embedded in wallboards, roofs, and floors of structures. Kong et al. [8] noted a significant reduction of system space temperature by about 2.4°C with SSPCM-integrated wallboard. Similarly, Lee et al. [9] noted a decrease in the heat influx of residential space by 25% when the walls were integrated with PCM and insulation mixture. In addition, Biswas et al. [10] studied the effect of NanoPCM integrated wallboard with graphite nano-sheets and noted a decrement by 25% in yearly heat gain of the system space. Further, granulated organic paraffin PCM incorporated roofs studied by Kosny et al. [11], showed a promising reduction in the cooling load of a study room by 55%. Apart from their heat storage characteristics, PCMs are preferred because of reduced weight, enhanced compatibility, and passivity compared to typical heat sink alternatives.

PCMs are categorized into many types, the most common of which are organic and inorganic PCMs. Salt hydrate is one such example of a frequently used inorganic PCM. Metallic PCMs present themselves as better inorganic PCMs with enhanced thermal conductivity and stability at the expense of increased weight that hinders their practicality in certain applications [12]. Fig. 1 [13] shows the stages of phase transition in PCMs.

* Corresponding author.
E-mail address: morhan@aus.edu (M.F. Orhan).

https://doi.org/10.1016/j.ijft.2022.100201

Available online 30 August 2022

Nomenclature

A_s	Heat transfer surface area (m^2)
b	Coefficient of volume expansion (1/K)
C_p	Specific heat (kJ/kg.K)
g	Gravitational acceleration (m/s^2)
h	The average heat transfer coefficient. ($W/m^2.K$)
k	Thermal conductivity (W/m. K)
L	Specific latent heat of the PCM (J/g).
L_c	Characteristic length of the geometry (m)
m	Mass (kg)
m_{PCM}	The mass of PCM (g).
υ	Kinematic viscosity of the fluid (m^2/s)
T∞	Temperature of the surrounding air (°C)
Ts	Temperature of the surface (°C)
GnPs	Graphene Nanoplatelets
PCM	Phase change material
SDBS	Sodium Dodecylbenzene Sulfonate
SDS	Sodium Dodecyl Sulfate
SSL	Sodium Stearoyl Lactylate

Subscripts

Al	Aluminum
Conv	Convection
l	Liquid
pcm	Phase change material
s	Solid

As far as organic PCMs are concerned, petroleum-based PCMs are an attractive choice and are suitable for a variety of different applications. From Table 1 [14–20], amongst the two types of PCMs in comparison, organic PCMs have various favorable qualities with fewer drawbacks.

Although organic PCMs have high stability, high latent heat density, and compatibility, their thermal conductivity seems to be the biggest drawback, as evident in Table 1. Poor thermal conductivity hinders the ability of the material to conduct heat leading to inefficient absorption of heat and low heat utilization efficiency for the system, which limits their utilization [21]. Many researchers have invested considerable efforts to find methods towards enhancing the thermal conductivity of PCMs. One such technique is the addition of conductive additives that are able to improve the thermal conductivity through forming a PCM composite. However, there are a variety of different additives and PCM mixtures that can be utilized, as well as different techniques of mixture formation.

Efforts have been made to implement graphite [22, 23], carbon fiber [24], and nanomaterials [25–27] into a water tank filled with a PCM to enhance the thermal properties of the system. Parlak et al. [28] combined an organic petroleum-based PCM, paraffin wax, with Graphene nanoplatelets at different mass fractions range of 0–10%. Adding a 10% mass fraction of Graphene Nanoplatelets improved thermal conductivity by 300%. Furthermore, Temel et al. [29] evaluated heating performances of petroleum-based PCM/GnPs composites at various mass fractions. It was illustrated that the thermal conductivity of the PCM increased by 253% when mixed with GnPs at 7% mass fractions. Also, Mehrali et al. [30] investigated the effects of a palmitic acid/GnPs composite, formed by a vacuum impregnation, on shape stability and thermal conductivity and revealed a total of 630% improvement in the thermal conductivity of the PCM. However, mixing the GnPs and the base PCM together may cause the accumulation of clumps that reduce the PCM's thermal conductivity. Therefore, through the use of ultrasonic techniques and the utilization of surfactants.

Table 1
Comparison of common types of phase change materials [14–20].

Type	Advantages	Disadvantages
Inorganic	High thermal conductivity	Lack of thermal & chemical stability
	High latent heat storage capacity	Prone to corrosion
	Low material cost	Exhibits supercooling phenomena
Organic	Chemical and thermal stability	Low thermal conductivity
	High latent heat density	Inflammable
	Large range of phase change temperatures	Relatively larger volume change

Even though it improves thermal conductivity, the addition of Graphene Nanoplatelets into organic PCMs results in poor stability and reduced thermal performance due to aggregation and sedimentation [37, 60]. To neutralize this effect, studies suggested the addition of chemical substances called surfactants. Surfactants are composed of amphipathic molecules that utilize electrostatic stabilization through adjusting the surface charge of the nanoparticles causing appropriate dispersion of these additives in organic PCMs [37]. Table 2 [31–58] summarizes the attempts made in different studies that include the addition of various surfactants in different mixtures of fluids and nanoparticle composites. Zhang et al. [59] added multiwall carbon nano-tube (MWCNT) particles to n-hexadecane to reduce supercooling. However, an aggregation of the MWCNT particles reduced its effectiveness. On the other hand, through the addition of strong acids such as H2SO4 and HNO3 as well as 1-decanol of surfactant to the MWCNT particles, the mixture was able to reduce supercooling through effective

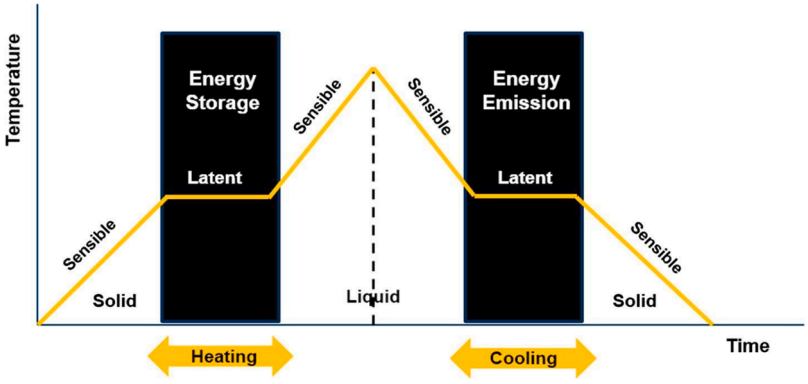

Fig. 1. Stages of phase transition in PCMs [13].

Table 2
Application of surfactants in different types of mixtures [31–58].

Author	Base Fluid	Nanoparticles	Surfactant
Xian et al. [31]	Distilled water and Ethylene Glycol	Graphene Nanoplatelets (GnPs)	PVP, Triton X-100, SDS, SDC, SDBS, and CTAB
Zhai et al. [32]	Ethylene Glycol	Aluminum oxide (Al_2O_3)	PVP, and SDS
Ordóñez et al. [33]	Deionized Water	Zirconium oxide (ZrO_2)	SDBS, CTAB, and PVP
Almanassra et al. [34]	Water	Multi-wall carbon nanotubes (MWCNT)	GA, SDS, and PVP
Gallego et al. [35]	Water	Aluminum oxide (Al_2O_3)	SDBS
Nourani et al. [36]	Paraffin	Aluminum oxide (Al_2O_3)	SSL
Cacua et al. [37]	Deionized Water	Aluminum oxide (Al2O3)	SDBS, and CTAB
Madni et al. [38]	Dimethyl Formamide	Multiwalled carbon nanotubes (MWNTs)	DTAB, and SOCT
Al-Waeli et al. [39]	Water	Silicon carbide (SiC)	SDS, SDBS, CTAB, and SDC
Asadi et al. [40]	Distilled water	Magnesium Hydroxide $Mg(OH)_2$	CTAB, SDS, and Oleic Acid
Das et al. [41]	Distilled water	Aluminum oxide (Al_2O_3)	CTAB, SDS, and SDBS
Gimeno-Furio et al. [42]	Eutectic mixture	Carbon-based nanoparticles	SDS, SDBS, and DS
Singh et al. [43]	Therminol 59 and Therminol 66	Copper (Cu)	BAC, and ODT
Wei et al. [44]	Diathermic oil	Silicon carbide (SiC), and titanium dioxide (TiO_2)	Oleic acid
Sarsam et al. [45]	Water	Graphene Nanoplatelets (GnPs)	SDS, SDBS, GA, and CTAB
Silakhori et al. [46]	Palmitic acid	Graphene Nanoplatelets (GnPs)	SDS
Yousefi et al. [47]	Distilled water	Aluminum oxide	Triton X-100
Yousefi et al. [48]	Distilled water	Multi-wall carbon nanotubes (MWCNT)	Triton X-100
Shojaeizadeh and Veysi [49]	Water	Aluminum oxide	SDBS
Said et al. [50]	Water	Titanium dioxide	PEG
Verma et al. [51]	Water	Graphene	Triton X-100
Said et al. [52]	Water	Single Wall Carbon Nanotubes	SDS
Gan et al. [53]	Water	Titanium dioxide	PVP
Sami and Etesami [54]	Paraffin	Titanium oxide	SSL
Ho and Gao [55]	N-octadecane	Aluminum oxide	Non-ionic
Li et al. [56]	ethylene glycol	Zinc oxide	PVP
Rufus et al. [57]	Paraffin	Graphene oxide	SDBS
Zeng et al. [58]	Palmitic acid	Multi-walled carbon nanotubes	CTAB, and SDBS

SDBS: Sodium dodecylbenzene sulfonate, CTAB: Cetyltrimethylammonium bromide, SDS: Sodium dodecyl sulfate, GA: Gum Arabic, PVP: Polyvinylpyrrolidone, SDC: Sodium deoxycholate, SSL: sodium stearoyl lactylate, DTAB: Dodecyl trimethylammonium bromide, SOCT: Sodium octanoate, DS: Diphenyl sulfone, ODT: Octadecyl thiol, BAC: benzalkonium chloride, PEG: Polyethylene glycol.

dispersion of the MWCNT particles. Choi et al. [60] investigated the effect of carbon additives on the thermal conductivity of a PCM and used Poly Vinyl Pyrrolidone (PVP) as a surfactant to enhance dispersion stability; as a result, the aggregation was reduced, and the thermal management capabilities of the system were improved

To our best knowledge from the aforementioned extensive literature review, no study has been conducted examining the effectiveness of thermal characteristic enhancement through the addition of graphene nanoplatelet (GnPs) in bio-based PCM produced by PureTemp Company. Therefore, to fill this gap, our objectives in this study are to thoroughly investigate the cooling characteristics of graphene nanoplatelet embedded in surfactants induced PCM as a heat sink for a heat source. The surfactants used for enhancing the thermal stability of the composite are sodium dodecyl sulfate (SDS), sodium dodecyl benzenesulfonate (SDBS), and sodium stearoyl lactylate (SSL). Also, to measure the thermal characteristics in terms of indices such as thermal conductivity, thermal capacity, and time of reaching the reference temperature. Furthermore, to carry out an intensive parametric study and optimize the constituents of the composite PCM for the best thermal characteristics.

2. Materials and methods

2.1. Materials

The bio-based PCM utilized in the following experiment is attained from Entropy Solutions, LLC. The PCM has a melting temperature of 29°C with a latent heat of melting of 202 kJ, as summarized in Table 3. The table contains the key thermal properties of the bio-based PCM used in the experiment. The Graphene Nanoplatelets (Grade M) additive was supplied by XGScience and is used to enhance the thermal conductivity of the bio-based PCM. Table 4 summarizes the thermal properties of the selected Graphene Nanoplatelet (GnPs). Upon comparing the effective change in thermal conductivity due to the addition of GnPs, results revealed that the addition of GnPs largely enhances the thermal conductivity of the Graphene Nanoplatelets-PCM composite (NanoPCM).

2.2. Preparation of GnPs/bio-based PCM composites

The PCM is initially solid and needs to be melted to liquid form to mix with the GNP. Next, a set of surfactants are added to the NanoPCM mixture namely, sodium dodecyl sulfate (SDS), Sodium dodecylbenzene sulfonate (SDBS), and Sodium stearoyl lactylate (SSL). To provide a sufficiently homogenous substance, the mixture is exposed to ultrasonic waves through a probe sonicator for 20 min. The mixture is placed in a beaker and is subjected to a 500 W QSonica sonicator at 25% amplitude. Finally, it is placed in a container to cool down and solidify at room temperature.

2.3. Thermal conductivity measurement

A thermal conductivity analyzer from C-Therm Technologies is utilized to measure the thermal conductivity of the samples of the pure bio-based PCM and Nano-PCM with different surfactants. The measurements are taken at room temperature (25°C). Heat loss due to convection affects the results; therefore, the thermal conductivity of a small test cell with a small volume is measured to minimize this effect. The test cell is placed on the sensor to take the readings, as visible in Fig. 2, after the sample is solidified.

2.4. Latent heat measurement

The latent heat of each sample impacts thermal management capabilities and therefore must be measured. In this regard, a Differential Scanning Calorimeter (DSC- 60a Plus, Shimadzu) is employed. The

Table 3
Thermal properties of PureTemp 29.

Property	Typical value
Melting temperature	29 °C
Latent heat, melting	202 kJ/kg
Specific heat capacity (solid)	1.77 kJ/(kg • °C)
Specific heat capacity (liquid)	1.94 kJ/(kg • °C)
Thermal conductivity (solid)	0.25 W/(m • °C)
Thermal conductivity (liquid)	0.15 W/(m • °C)
Density at 6 °C (solid)	0.94 g/cm^3
Density at 30 °C (liquid)	0.85 g/cm^3

Table 4
Key thermal properties of graphene nanoplatelets.

Property	Typical value (perpendicular to the surface)
Density	2.2 g/cm^3
Thermal conductivity	6 W/(m • °C)
Specific heat capacity	2.1 kJ/(kg • °C)

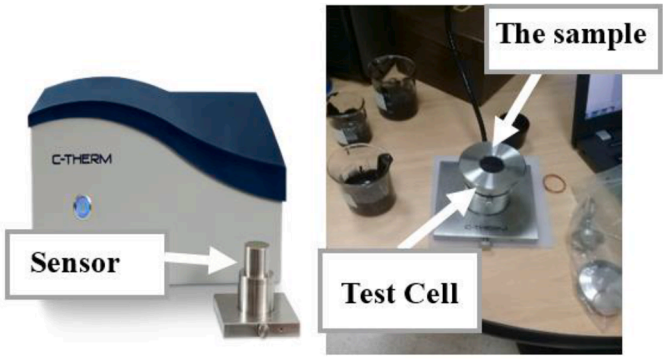

Fig. 2. C-Therm Thermal Conductivity Analyzer.

latent heat of the four samples including the pure PCM are analyzed and compared using the DSC analysis. Through this comparison process, the effect of each surfactant on the latent heat is evaluated using an initial reference temperature of 24°C in all samples. The samples are then heated at a rate of 1°C/min until a temperature of 45°C is achieved. Any endothermic melting process is carefully noted. Finally, results from the DSC analysis are plotted in a heat vs time graph for each sample.

2.5. Experimental setup

Once the latent heat and the thermal conductivity are calculated for each sample, then their performance is evaluated. As seen in Fig. 3, the NanoPCM surfactant mixture is used as a heat sink and tested using the TecQuipment Free and Forced Convection Experimental Apparatus. The setup is used to measure the heater surface temperature. The heated surface on the setup with dimensions of 106×106×3 mm^3 dissipates heat to the aluminum container consisting of a 30 mL mixture. The temperature is measured using a thermocouple placed on the aluminum plate where the mixture container is kept. The heater is set to 10 W, which is directly transmitted to the plate. The temperature, as well as the time, are recorded using a data acquisition system.

A schematic diagram of a cross-section of the PCM-based heat sink is presented in Fig. 4. A constant heat flux of 943W/m^2 is applied to the bottom wall of the plate.

2.6. Measurement error analysis

As illustrated in Table 5, the resolution of each instrument is adequately accurate and the error values do not cause any validation issues. The heaters are the least accurate component, however, the heaters in such experimental setups do not require high accuracy. The ther-mo-cou-ple and the bal-ance mea-sure data with high accu-racy, good res-o-lu-tion, and minor un-cer-tain-ties.. The TecQuipment free and forced convection experiment provided sufficient accuracy as 0.2°C temperature uncertainty maintain validity and integrity of temperature data.

3. Results and discussion

This section presents and discusses the results obtained from the thermal conductivity and thermal performance experiments of NanoPCM composites as well as PurePCM (bio-based). Experiments are conducted on three separate mass fractions of GnPs, i.e., 1%, 3%, and 5%. Moreover, all experimented samples containe a steady 1:1 GnPs to surfactant ratio. Furthermore, as highlighted in previous sections, three separate surfactants are used namely, SDBS, SDS, and SSL.

3.1. Thermal conductivity of surfactant induced NanoPCM composites

Fig. 5 summarizes the results extracted from thermal conductivity experiments conducted on NanoPCM samples containing each of three surfactant variants of 1%, 3%, and 5% mass fractions of GnPs.

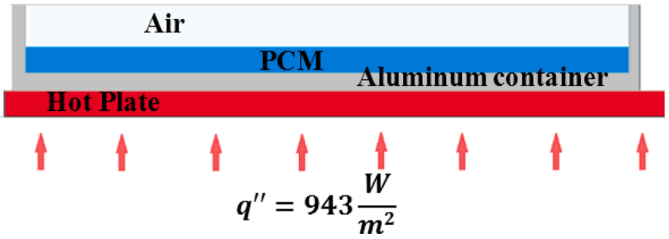

Fig. 4. Schematic diagram of a cross-section of PCM-based heat sink.

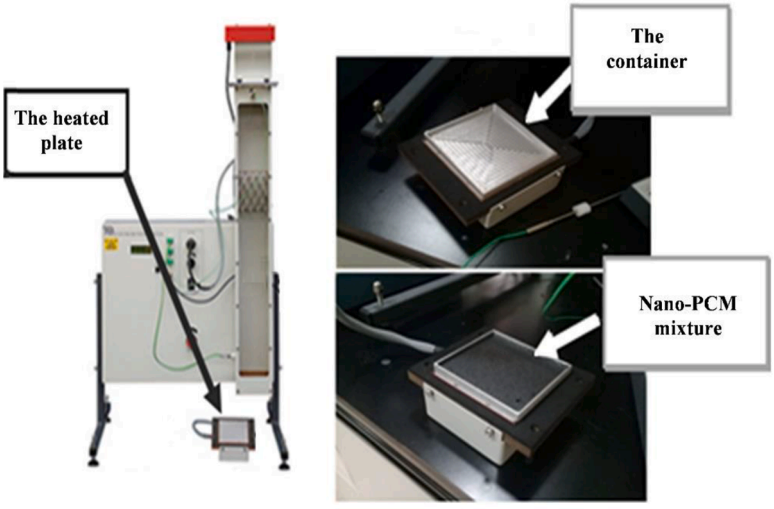

Fig. 3. Experimental Apparatus.

Table 5
Instrument uncertainty.

Instrument	Uncertainty	Deviation
C-Therm TCi thermal conductivity analyzer	±0.01 W/ m K	0.02 W/ m K
Q500 QSonica sonicator	–	1 W
Citizen CX220 Analytical Balance	±0.1 mg	0.1 mg
TecQuipment experiment (Heater) [Model: TD1005]	±0.1 W	0.1 W
TecQuipment experiment (Thermocouple) [Model: TD1005]	±0.2 °C	0.1 °C
Shimadzu DSC-60a Plus	±0.01 mW	0.01 mW

Furthermore, an additional 0% GnPs mass fraction bar has been added to Fig. 5 to compare the thermal conductivity results with that of the PurePCM sample.

As shown in Fig. 5, the thermal conductivity of 0.22W/m.K is measured for the PurePCM sample. In the case of the GnPs-Surfactant mixed PCM samples, a significant increase in the thermal conductivity is achieved comparing to the PurePCM sample. The maximum thermal conductivity values of 0.54, 0.79 and 1.03W/m.K are measured for 1, 3, and 5% GnPs mass fractions, respectively. These maximum thermal conductivity values represent a percentage increase of approximately 150, 260, and 370% for the 1, 3, and 5% GnPs mass fractions, respectively when compared to the PurePCM sample. Thus, it is found that a significant improvement in the thermal conductivity of PurePCM can be achieved by the incorporation of a GnPs-Surfactant mixture within the PurePCM sample. Furthermore, the figure also confirms that in all cases (1, 3, and 5% GnPs mass fractions), the NanoPCM-SDS sample generates the highest thermal conductivity measurement and thus it appears to be the most suitable choice when thermal conductivity is considered.

In addition, Fig. 5 also shows that amongst the three GnPs mass fractions in evaluation, 5% GnPs mass fraction reported the highest thermal conductivity measurement for all types of surfactants. In comparison to 1 and 3% GnPs mass fraction NanoPCM-SDS, 5% GnPs NanoPCM-SDS yields a thermal conductivity percentage increase of 89% against its 1% counterpart and a percentage increase of 30% against its 3% counterpart.

Thus, when thermal conductivity is considered the current experiment finds that amongst the studied samples, 5% GnPs mass fraction NanoPCM-SDS reports the highest thermal conductivity measurement.

3.2. DSC analysis of surfactant induced NanoPCM composites

Figs. 6, 7, and 8 describe the thermal capacity at each temperature during the DSC analysis for the 1, 3, and 5% GnPs mass fraction NanoPCM samples, respectively, when the three different surfactants are used. Given that the thermal capacity is described in J/g, the same parameter against the temperature curve is also representative of the specific heat, annotated as C_p for the measured sample. Measurements are carried out using the DSC-60a Plus, Shimadzu Differential Scanning Calorimeter where samples are placed at an initial temperature of 24°C and then heated to 35°C, steadily at a rate of 1°C/min. In the case of all three mass fraction variants, the endothermic process is carefully analyzed. Furthermore, a DSC analysis is also carried out for PurePCM samples thereby serving as a control sample.

The phase change temperature for all measured samples is considered to be in an approximate range of 27 to 29°C, where the thermal capacity of each sample shows a sharp rise as a result of the phase-change process. The difference in the phase change temperature

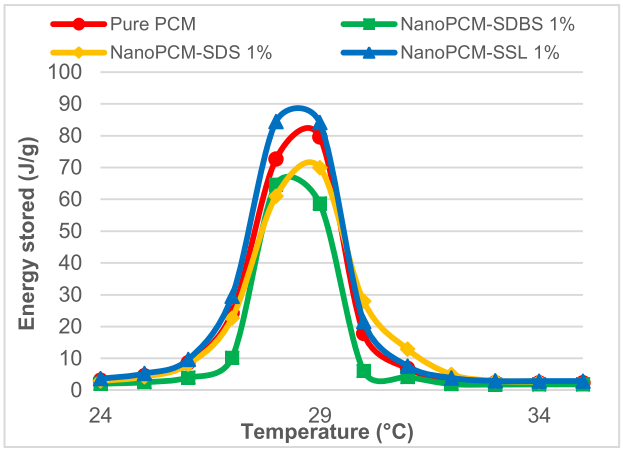

Fig. 6. Thermal capacity against temperature for 1% GnPs mass fraction.

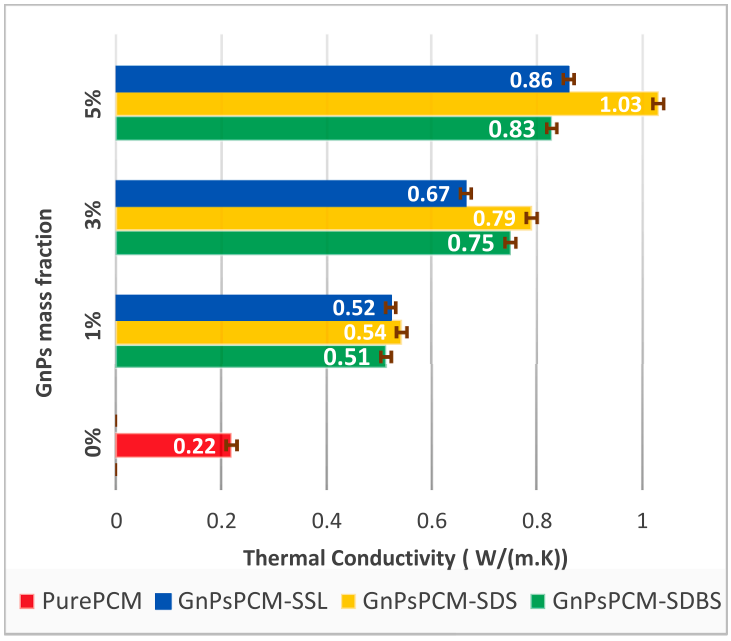

Fig. 5. Thermal conductivity values of NanoPCM with various mass fractions of GnPs.

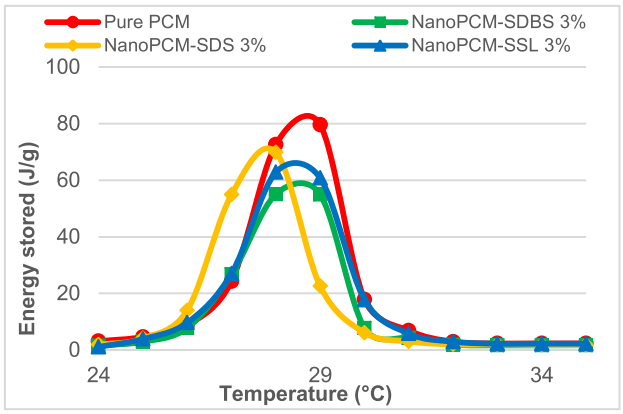

Fig. 7. Thermal capacity against temperature for 3% GnPs mass fraction.

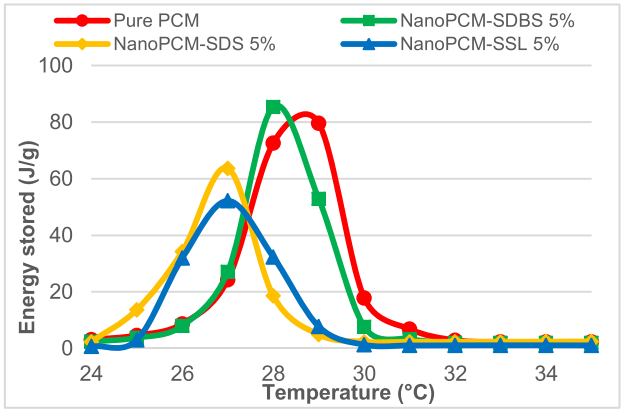

Fig. 8. Thermal capacity against temperature for 5% GnPs mass fraction.

amongst samples is associated with varying GnPs mass fractions as well as the type of surfactant.

From Fig. 6, in the case of 1% GnPs mass fraction, thermal capacity appears to peak at approximately 28–29°C. This trend is observed for all measured surfactants. The phase change region spans from approximately 25 to 32°C. In terms of the peak thermal capacity, NanoPCM-SSL shows the highest peak energy storage of approximately 88 J/g, while NanoPCM-SDBS demonstrates the lowest peak thermal capacity of approximately 67 J/g.

Fig. 7 illustrates that, in the case of 3% GnPs mass fraction, thermal capacity appears to peak at approximately 27–29°C. This trend is observed for all measured surfactants. For 1% GnPs mass fraction, the phase change region spans from approximately 25 to 32°C. For the peak thermal capacity amongst measured surfactant induced NanoPCM samples, NanoPCM-SDS shows the highest peak thermal capacity of approximately 70J/g, while NanoPCM-SDBS demonstrates the lowest peak thermal capacity of approximately 57J/g. In the current case, PurePCM measures a taller thermal capacity peak when compared to the NanoPCM-Surfactant samples.

As observed from Fig. 8, in the case of 5% GnPs mass fraction, thermal capacity peaks at approximately 27–29°C, which is observed for all measured surfactants. The phase change region spans from approximately 24 to 32°C. Regarding the peak thermal capacity, NanoPCM-SDBS illustrates the highest peak thermal capacity of approximately 85J/g. On the other hand, NanoPCM-SSL demonstrates the lowest peak thermal capacity of approximately 51J/g.

In the comparisons of Figs. 6, 7, and 8, it is observed that the highest peak thermal capacity is demonstrated by 1% NanoPCM-SSL and followed closely by 5% NanoPCM-SDBS, while the lowest peak thermal capacity is represented by 5% NanoPCM-SSL.

The total phase change enthalpy of all samples is summarized in Fig. 9. The total phase change enthalpy is acquired by the addition of thermal capacity in the entire phase change region. In the current experiment, samples exhibit a phase change region in the range of 24 to 31°C, with slight variations based on the GnPs mass fraction and surfactant used.

As shown in Fig. 9 PurePCM (represented by 0% GnPs mass fraction) yields a final phase change enthalpy of 212.2J/g. With the exception of 1% NanoPCM-SSL, all other measured samples produce a phase change enthalpy value lower than that of PurePCM. 1% NanoPCM-SSL measures the maximum phase change enthalpy of 236.5J/g, which is approximately an 11.5% increase in phase change enthalpy in comparison to PurePCM. The lowest phase change enthalpy is attributed to 5% NanoPCM-SSL that exhibits a phase change enthalpy of 128.12J/g, a 40% decrease when compared against PurePCM. Thus when phase change enthalpy is considered, 1% NanoPCM-SSL appears to demonstrate the largest capacity to absorb energy at a constant temperature and thus may perform the best when cooling applications are considered.

From Fig. 9, noteworthy trends are observed when the relationship between GnPs mass fraction and Surfactant is considered. In the case of 1, 3, and 5% NanoPCM-SSL phase change enthalpies are found to be 236.5, 197.7, and 128.12J/g, respectively. 1, 3, and 5% NanoPCM-SDS show a similar trend with phase change enthalpies of 206.7, 167.4, and 147.3J/g, respectively. Thus, in the case of SSL and SDS surfactants, phase change enthalpy appears to decrease at larger GnPs mass fractions. On the contrary, 1, 3, and 5% NanoPCM-SDBS produce phase change values of 145.9, 161.8, and 185.5J/g, respectively. Thus, the SDBS surfactant demonstrates an opposite effect where phase change enthalpy appears to increase when GnPs mass fraction rises.

3.3. The thermal performance of surfactant-induced NanoPCM composites

Figs. 10, 11, and 12 illustrate the thermal performance of 1, 3, and 5% GnPs mass fraction NanoPCM samples with three different surfactants. In each case, the thermal response of PurePCM is also studied alongside the NanoPCM-Surfactant samples. In the figures, the thermal performance is represented in the form of varying transient thermal responses of a 10W heater when the GnPs-Surfactant integrated PCM is utilized as a heat sink. Each experiment is carried out for a fixed time period (approx. 900s), thereby, ensuring high comparability when results are analyzed. The focal point of the experiment is the final temperature of the heating element. Lower final temperatures represent the superior thermal performance of the heat sink as it indicates that the material is able to absorb a higher amount of heat within the given timeframe.

As evident from Figs. 10-12, PurePCM exhibits a final temperature of 44.8 ℃ at the end of the 900-second period. In comparison to the NanoPCM-Surfactant final temperatures for different GnPs mass fractions, Fig. 10 confirms that in the case of all three surfactants, 1% GnPs mass fraction NanoPCM-Surfactant samples exhibit a final temperature lower than that of PurePCM with a minimum temperature of 44.1 ℃ attributed to the NanoPCM-SSL sample. Figs. 11 and 12 present a similar trend for the 3 and 5% GnPs mass fractions where all the three surfactant variants exhibit lower final temperatures than the PurePCM. The minimum final temperatures of 42.9 and 42.2 ℃ are recorded for 3 and 5% GnPs mass fractions, respectively. Similar to 1% mass fraction, 3 and 5% GnPs mass fraction samples also attribute their minimum final temperatures to the NanoPCM-SSL sample variant. Therefore, it is possible to infer that in all three cases of GnPs mass fractions that are studied, the integration of a GnPs-Surfactant mixture within the PurePCM augments the thermal performance of the PCM heat sink. Furthermore, all three GnPs mass fraction samples show that, amongst the three tested surfactant variants, the NanoPCM-SSL variant appears to have the most superior heat transfer characteristics. However, as seen in Fig. 12,

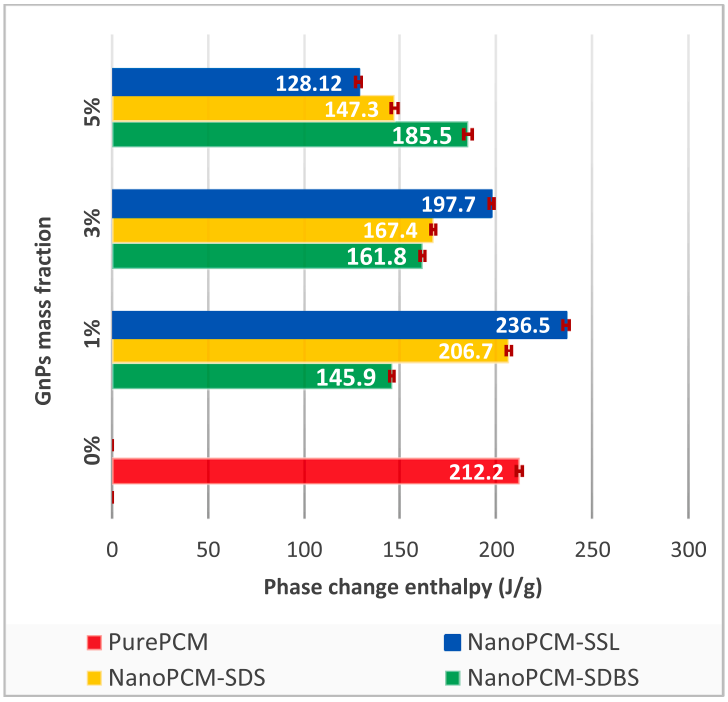

Fig. 9. Phase change enthalpy values for different GnPs mass fractions.

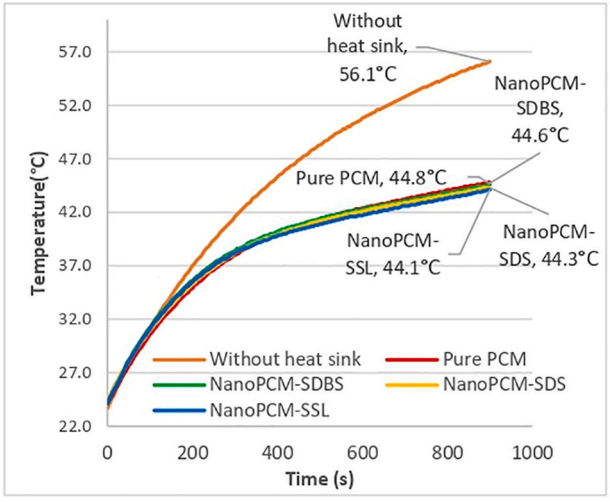

Fig. 10. Increase in temperature against time for surfactant embedded NanoPCM as heat sink at 1% mass fraction of GnPs.

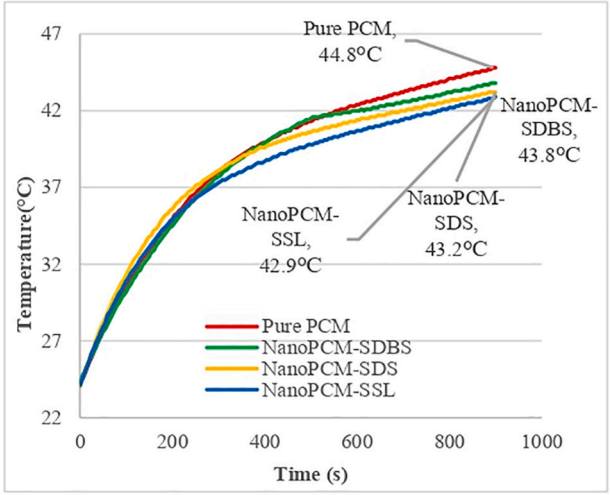

Fig. 11. Increase in temperature against time for surfactant embedded NanoPCM as heat sink at 3% mass fraction of GnPs.

NanoPCM-SSL at 5% mass fraction exhibits the lowest overall temperature of 42.2 ℃ at the end of the 900 second period. Thus, it is important to notice the effect of adding different mass fractions of the GnPs-surfactant mixture with a 1:1 ratio. Figs. 10, 11, and 12 illustrate how the temperature of the NanoPCM mixed with SDS, SDBS, and SSL decrease with larger mass fractions at the end of the allocated time.

The time taken for a hot plate to reach a fixed temperature serves as an important parameter in the evaluation of the cooling performance of a substance. In this regard, Fig. 13 highlights a magnified portion of the varying transient thermal response of the heater for 1% GnPs mass fraction. A horizontal line (highlighted in gray) is plotted at the reference temperature in consideration, 43 ℃ in the current experiment. The time taken for each sample to reach this reference temperature is then evaluated using vertical lines. Longer durations in the figure indicate the superior cooling performance of the heat sink. A similar method is employed for 0 (PurePCM), 3, and 5% mass fractions, as illustrated in Fig. 14.

In Fig. 14, PurePCM takes 670 s to reach the reference temperature of 43℃. In comparison to the NanoPCM-Surfactant for the 1% GnPs mass fraction, Fig. 14 confirms that in all three surfactant cases (SDBS, SSL, and SDS) a longer time is observed, with a maximum of 760 s attributed to the NanoPCM-SSL sample. Similar trends are observed in the case of the remaining two mass fractions where the NanoPCM-SSL variant measures a maximum time of 910 and 1015 s for the 3 and 5% fractions, respectively. Therefore, in comparison to the PurePCM, a 13, 35, and 51% more duration is observed for 1, 3, and 5% GnPs mass fractions, respectively.

Fig. 14 presents the effect of 1, 3, and 5% mass fractions on the time required to reach the reference temperature of 43 ℃. NanoPCM-SSL with a 5% GnPs-surfactant mixture illustrates the longest time of

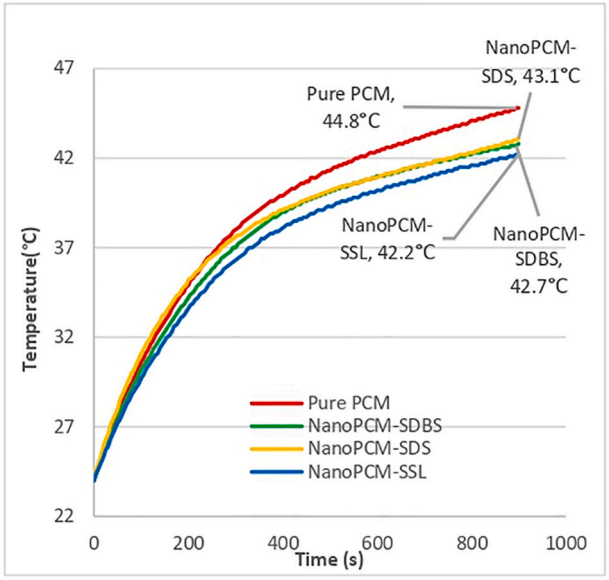

Fig. 12. Increase in temperature against time for surfactant embedded NanoPCM as heat sink at 5% mass fraction of GnPs.

1015 s, while pure PCM displays the shortest time of 670 s. Therefore, the duration of achieving the reference temperature increases at larger mass fractions; 695, 770 and 935 s for 1, 3 and 5% NanoPCM-SDBS, respectively. NanoPCM-SDS and NanoPCM-SSL follow a similar trend of longer durations at larger mass fractions, which clearly portray the relationship between transient time and the mass fraction of the GnPs-surfactant mixture.

3.4. Heat transfer analysis of PCM based heat sink

The net rate of heat absorbed by a PCM is the summation of the sensible heat of the PCM in both the solid and liquid phases, and the latent heat in the transition phase. This relation is formulated in Eq. (1) as,

$$\dot{Q}_{pcm} = \frac{m_{pcm} c_{p,s}\ \Delta T\ + m_{pcm} L + m_{pcm}\ c_{p,l}\ \Delta T}{\Delta t} \tag{1}$$

where, m_{pcm} is the mass of the PCM, c_p is the specific heat capacity of the substance, ΔT is the change in temperature, and Δt is the change in time. The rate of heat absorbed by the aluminum container is calculated by using the following equation,

$$\dot{Q}_{Al} = m_{Al} c_{p,Al}\ \Delta T \tag{2}$$

where, $m_{Al}$and $c_{p,Al}$ represent the mass and specific heat capacity of aluminum, respectively. The rate of heat transfer by natural convection is calculated using Newton's law of cooling, as the following equation,

$$\dot{Q}_{conv} = h\ A_s (T_s - T_\infty) \tag{3}$$

where, A_s is the heat transfer surface area, T_s is the temperature of the surface, and T_∞ is the temperature of the surrounding air which is measured as 24 ℃. The heat transfer coefficient, annotated as h, in the above equation, is calculated using the following equation,

$$h = \frac{k}{L_c} \tag{4}$$

where, k represents the thermal conductivity, and Lc is the characteristic length of the geometry. The Nusselt number is calculated by the following equation for the horizontal plate where heat transfer occurs in an upward direction [61],

$$Nu = 0.27 Ra_L^{\frac{1}{4}} \tag{5}$$

The Nusselt number for the vertical plate is calculated as [61],

$$Nu = \left\{ 0.825 + \frac{0.387 Ra_L^{\frac{1}{6}}}{\left[1 + (0.492/Pr)^{9/16}\right]^{8/27}} \right\}^2 \tag{6}$$

The Rayleigh number (*Ra*) that is obtained through the product of Prandtl number (Pr) and Grashof number is calculated as [61],

$$Ra_L = \frac{g\beta\ (T_s - T_\infty) {L_c}^3}{\upsilon^2}\ Pr \tag{7}$$

where, *g*, β, *υ* represent the gravitational acceleration, the coefficient of volume expansion, the kinematic viscosity, respectively. Using the equations above, the results are graphically summarized in Fig. 15. The pie chart in the figure describes the percentage share of each component in the control system responsible for heat transfer. In a fixed time interval, pure PCM absorbs 60% of the heat from the source. The surrounding convective conditions on the very top of the PCM are responsible for absorbing 4% of the heat transmitted from the source. A minor share of the heat, amounting to 8%, is absorbed by the aluminum container.

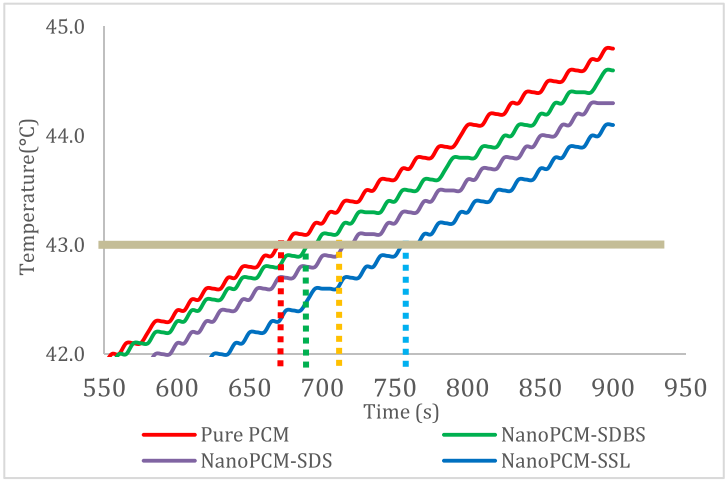

Fig. 13. Duration to reach the reference temperature for surfactant embedded NanoPCM as a heat sink for 1% mass fraction of GnPs.

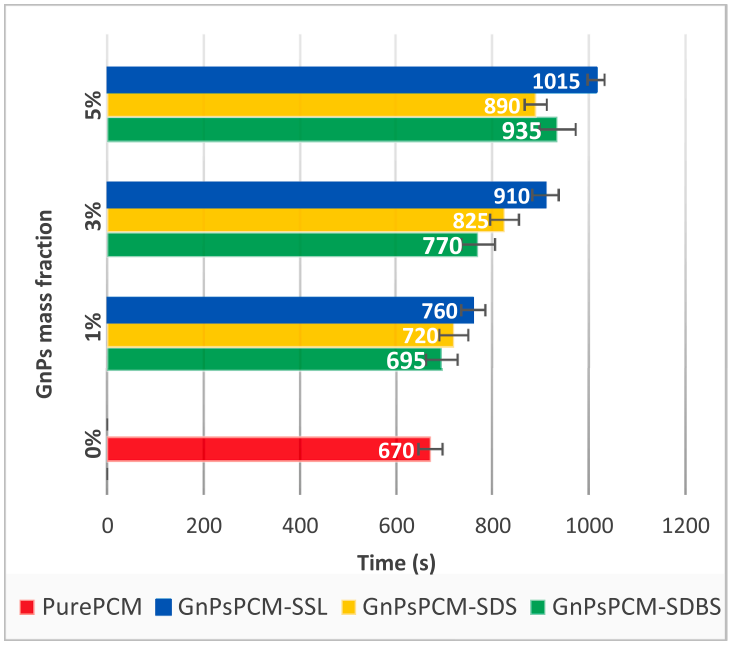

Fig. 14. Duration to reach the reference temperature for surfactant embedded NanoPCM.

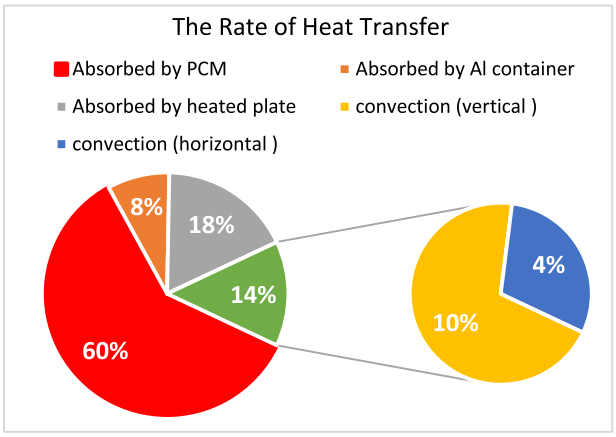

Fig. 15. Heat transfer analysis of PCM based heat sink.

4. Conclusion

In this study, the cooling characteristics of PurePCM embedded with conductive additives and surfactants to enhance thermal conductivity and chemical stability at high temperatures have been presented. Cooling characteristics have been measured through indices such as thermal conductivity, thermal energy capacity for a variety of temperatures, phase change enthalpy, and time taken to reach the reference temperature. In addition to varying the mass fractions of GnPs at 1, 3, and 5% of the mixture, several surfactants namely sodium dodecyl sulfate, sodium dodecylbenzene sulfonate, and sodium stearoyl lactylate have been studied for their thermal properties. The extensive experimental study and analysis allow several conclusions to be drawn. Among all test samples, the highest thermal conductivity is recorded at 5% GnPs mass fraction for all three surfactants. NanoPCM-SDS has a thermal conductivity of 1.03W/m.K in comparison to that of 0.22W/m.K for the PurePCM, which substantiates the need for conductive-additives into the PurePCM. The conductive and surfactant-induced composite reaches a peaky thermal energy capacity at about 29°C, melting temperature of PurePCM. The most promising phase change enthalpy per unit weight is obtained at 1% GnPs mass fraction for NanoPCM-SSL amounting to 236.5J/g. The highest values for NanoPCM-SDS are noted at 1% GnPs mass fraction, while 5% for NanoPCM-SDBS. Furthermore, NanoPCM-SDS at 5% GnPs mass fraction displays superiority in terms of thermal conductivity closely followed by NanoPCM-SSL. In terms of thermal capacity and time taken to reach the reference temperature of 43°C, NanoPCM-SSL at 1 and 5% mass fraction of GnPs, respectively, outperform the other samples. Finally, in terms of heat losses, 60% of the heat is transmitted from the source to the PurePCM while 8% is absorbed by the aluminum container casing and 14% is lost due to the surrounding convective conditions.

Declaration of Competing Interest

The authors declare that they have no known competing financial interests or personal relationships that could have appeared to influence the work reported in this paper.

Acknowledgments

We would like to express our gratitude to the late Professor Dr. Mohamed Gadalla for his assistance and support.

References

[1] K. Ochifuji, Y. Hamada, M. Nakamura, Thermal storage in Japan, in: Proceedings of Terrastock 8th International Conference of Thermal Energy Storage, Stuttgart, Germany, 2000, pp. 61–67.
[2] H. Mehling, L. Cabeza, Heat and Cold Storage With PCM (An Up to Date Introduction Into Basics and Applications), Springer, New York, 2008.
[3] G. Dogkas, et al., Investigating the performance of a thermal energy storage unit with paraffin as phase change material, targeting buildings' cooling needs: an experimental approach, Int. J. Thermofluids 3–4 (100027) (2020), 100027.
[4] M.K. Koukou, et al., Experimental assessment of a full scale prototype thermal energy storage tank using paraffin for space heating application, Int. J. Thermofluids 1–2 (100003) (2020), 100003.
[5] M. Rashad, N. Khordehgah, A. Żabnieńska-Góra, L. Ahmad, H. Jouhara, The utilisation of useful ambient energy in residential dwellings to improve thermal comfort and reduce energy consumption, Int. J. Thermofluids 9 (100059) (2021), 100059.
[6] C. Pagkalos, G. Dogkas, M.K. Koukou, J. Konstantaras, K. Lymperis, M. G. Vrachopoulos, Evaluation of water and paraffin PCM as storage media for use in thermal energy storage applications: a numerical approach, Int. J. Thermofluids 1–2 (100006) (2020), 100006.

[7] K. Azzouz, D. Leducq, D. Gobin, Enhancing the performance of household refrigerators with latent heat storage: an experimental investigation, Int. J. Refrig. 32 (2009) 1634–1644, https://doi.org/10.1016/j.ijrefrig.2009.03.012.

[8] X. Kong, C. Yao, P. Jie, Y. Liu, C. Qi, X. Rong, Development and thermal performance of an expanded perlite-based phase change material wallboard for passive cooling in building, Energy Build. 152 (2017) 547–557, https://doi.org/10.1016/j.enbuild.2017.06.067.

[9] K.O. Lee, M.A. Medina, X. Sun, X. Jin, Thermal performance of phase change materials (PCM)-enhanced cellulose insulation in passive solar residential building walls, Solar Energy 163 (2018) 113–121, https://doi.org/10.1016/j.solener.2018.01.086.

[10] K. Biswas, J. Lu, P. Soroushian, S. Shrestha, Combined experimental and numerical evaluation of a prototype nano-PCM enhanced wallboard, Appl. Energy 131 (2014), https://doi.org/10.1016/j.apenergy.2014.02.047.

[11] J. Kosny, K. Biswas, W. Miller, S. Kriner, Field thermal performance of naturally ventilated solar roof with PCM heat sink, Solar Energy 86 (2012) 2504–2514, https://doi.org/10.1016/j.solener.2012.05.020.

[12] B.R. Anupam, U.C. Sahoo, P. Rath, Phase change materials for pavement applications: a review, Construction and Build. Mater. 247 (2020), 118553, https://doi.org/10.1016/j.conbuildmat.2020.118553.

[13] R. Wen, W. Zhang, Z. Lv, Z. Huang, A novel composite PCM of Stearic Acid/Carbonized sunflower straw for thermal energy storage, Mater. Lett. 215 (2017), https://doi.org/10.1016/j.matlet.2017.12.008.

[14] A. Sharma, V.V. Tyagi, C.R. Chen, D. Buddhi, Review on thermal energy storage with phase change materials and applications, Renew. Sustain. Energy Rev. 13 (2) (2009) 318–345, https://doi.org/10.1016/j.rser.2007.10.005.

[15] B.E. Jebasingh, Thermal conductivity on ternary eutectic fatty acid as phase change material (PCM) by various treated exfoliated graphite nanoplatelets (xGnP, Front. Mater. Processing, Appl. Res. Technol. (2018) 75–84.

[16] M. Jourabian, M. Farhadi, Melting of nanoparticles-enhanced phase change material (NEPCM) in vertical semicircle enclosure: numerical study, J. Mech. Sci. Technol. 29 (9) (2015) 3819–3830, https://doi.org/10.1007/s12206-015-0828-0.

[17] B. Zalba, J.M. Mar4 n, L.F. Cabeza, H. Mehling, Review on thermal energy storage with phase change: materials, heat transfer analysis and applications, Appl. Therm. Eng. 23 (2003) 251–283.

[18] M. Kenisarin, High-temperature phase change materials for thermal energy storage, Renew. Sustain. Energy Rev. 14 (2010) 955–970, https://doi.org/10.1016/j.rser.2009.11.011.

[19] S. Khare, M. Dell'Amico, C. Knight, S. McGarry, Selection of materials for high temperature latent heat energy storage, Solar Energy Mater. Solar Cells 107 (2012) 20–27, https://doi.org/10.1016/j.solmat.2012.07.020.

[20] D. Zhou, C.Y. Zhao, Y. Tian, Review on thermal energy storage with phase change materials (PCMs) in building applications, Appl. Energy 92 (2012) 593–605, https://doi.org/10.1016/j.apenergy.2011.08.025.

[21] L. Xie, L. Tian, L. Yang, Y. Lv, Q. Li, Review on application of phase change material in water tanks, Adv. Mech. Eng. 9 (2017), https://doi.org/10.1177/1687814017703596.

[22] S. Pincemin, R. Olives, X. Py, M. Christ, Highly conductive composites made of phase change materials and graphite for thermal storage, Solar Energy Mater. Solar Cells 92 (6) (2008) 603–613, https://doi.org/10.1016/j.solmat.2007.11.010.

[23] X. Py, R. Olives, S. Mauran, Paraffin/porous-graphite matrix composite as a high and constant power thermal storage material, Int. J. Heat Mass Transf. 44 (2001) 2727–2737, https://doi.org/10.1016/S0017-9310(00)00309-4.

[24] J. Fukai, Y. Hamada, Y. Morozumi, O. Miyatake, Improvement of thermal characteristics of latent heat thermal energy storage units using carbon-fiber brushes: experiments and modeling, Int. J. Heat Mass Transf. 46 (2003) 4513–4525, https://doi.org/10.1016/S0017-9310(03)00290-4.

[25] X. Zhang, X.-.M. Tao, K.-.L. Yick, X.-c. Wang, Structure and thermal stability of microencapsulated phase-change materials, Colloid Polym. Sci. 282 (2004) 330–336, https://doi.org/10.1007/s00396-003-0925-y.

[26] J.M. Khodadadi, S.F. Hosseinizadeh, Nanoparticle-enhanced phase change materials (NEPCM) with great potential for improved thermal energy storage, Int. Commun. Heat and Mass Transf. 34 (5) (2007) 534–543.

[27] W. Li, X. Zhang, X.-.C. Wang, J.-.J. Niu, Preparation and characterization of microencapsulated phase change material with low remnant formaldehyde content," *Materials Chemistry and Physics*, Mater. Chem. Phys. 106 (2007) 437–442, https://doi.org/10.1016/j.matchemphys.2007.06.030.

[28] M. Parlak, K. Sömek, Ü.N. Temel, K. Yapici, Experimental investigation of transient thermal response of phase change material embedded by graphene nanoparticles in energy storage module, in: 2016 15th IEEE Intersociety Conference on Thermal and Thermomechanical Phenomena in Electronic Systems (ITherm), 2016, pp. 645–651, https://doi.org/10.1109/ITHERM.2016.7517609, 31 May-3 June 2016.

[29] U.N. Temel, K. Somek, M. Parlak, K. Yapici, Transient thermal response of phase change material embedded with graphene nanoplatelets in an energy storage unit, J. Therm. Anal. Calorim. 133 (2) (2018) 907–918, https://doi.org/10.1007/s10973-018-7161-7.

[30] M. Mehrali, et al., Preparation and characterization of palmitic acid/graphene nanoplatelets composite with remarkable thermal conductivity as a novel shape-stabilized phase change material, Appl. Therm. Eng. 61 (2013) 633–640, https://doi.org/10.1016/j.applthermaleng.2013.08.035.

[31] H.W. Xian, N.A.C. Sidik, R. Saidur, Impact of different surfactants and ultrasonication time on the stability and thermophysical properties of hybrid nanofluids, Int. Commun. Heat and Mass Transf. 110 (2020), 104389.

[32] Y. Zhai, L. Li, J. Wang, Z. Li, Evaluation of surfactant on stability and thermal performance of Al2O3-ethylene glycol (EG) nanofluids, Powder Technol. 343 (2019) 215–224.

[33] F. Ordóñez, F. Chejne, E. Pabón, K. Cacua, Synthesis of ZrO2 nanoparticles and effect of surfactant on dispersion and stability, Ceram. Int. 46 (8) (2020) 11970–11977.

[34] I.W. Almanassra, A.D. Manasrah, U.A. Al-Mubaiyedh, T. Al-Ansari, Z.O. Malaibari, M.A. Atieh, An experimental study on stability and thermal conductivity of water/CNTs nanofluids using different surfactants: a comparison study, J. Mol. Liq. 304 (2020), 111025.

[35] A. Gallego, K. Cacua, B. Herrera, D. Cabaleiro, M.M. Piñeiro, L. Lugo, Experimental evaluation of the effect in the stability and thermophysical properties of water-Al2O3 based nanofluids using SDBS as dispersant agent, Adv. Powder Technol. 31 (2) (2020) 560–570.

[36] M. Nourani, N. Hamdami, J. Keramat, A. Moheb, M. Shahedi, Thermal behavior of paraffin-nano-Al2O3 stabilized by sodium stearoyl lactylate as a stable phase change material with high thermal conductivity, Renew. Energy 88 (2016) 474–482.

[37] K. Cacua, F. Ordoñez, C. Zapata, B. Herrera, E. Pabón, R. Buitrago-Sierra, Surfactant concentration and pH effects on the zeta potential values of alumina nanofluids to inspect stability, Colloids and Surfaces A: Physicochem. Eng. Aspects 583 (2019), 123960.

[38] I. Madni, C.-.Y. Hwang, S.-.D. Park, Y.-.H. Choa, H.-.T. Kim, Mixed surfactant system for stable suspension of multiwalled carbon nanotubes, Colloids and Surfaces A: Physicochem. Eng. Aspects 358 (1–3) (2010) 101–107.

[39] A.H. Al-Waeli, M.T. Chaichan, H.A. Kazem, K. Sopian, Evaluation and analysis of nanofluid and surfactant impact on photovoltaic-thermal systems, Case Stud. Therm. Eng. 13 (2019), 100392.

[40] A. Asadi, M. Asadi, M. Siahmargoi, T. Asadi, M.G. Andarati, The effect of surfactant and sonication time on the stability and thermal conductivity of water-based nanofluid containing Mg(OH)2 nanoparticles: an experimental investigation, Int. J. Heat Mass Transf. 108 (2017) 191–198.

[41] P.K. Das, N. Islam, A.K. Santra, R. Ganguly, Experimental investigation of thermophysical properties of Al 2 O 3 –water nanofluid: role of surfactants, J. Mol. Liq. 237 (2017) 304–312.

[42] A. Gimeno-Furio, N. Navarrete, R. Mondragon, L. Hernandez, R. Martinez-Cuenca, L. Cabedo, J.E. Julia, Stabilization and characterization of a nanofluid based on a eutectic mixture of diphenyl and diphenyl oxide and carbon nanoparticles under high temperature conditions, Int. J. Heat Mass Transf. 113 (2017) 908–913.

[43] D. Singh, E.V. Timofeeva, M.R. Moravek, S. Cingarapu, W. Yu, T. Fischer, S. Mathur, Use of metallic nanoparticles to improve the thermophysical properties of organic heat transfer fluids used in concentrated solar power, Solar Energy 105 (2014) 468–478.

[44] B. Wei, C. Zou, X. Yuan, X. Li, Thermo-physical property evaluation of diathermic oil based hybrid nanofluids for heat transfer applications, Int. J. Heat Mass Transf. 107 (2017) 281–287.

[45] W.S. Sarsam, A. Amiri, S. Kazi, A. Badarudin, Stability and thermophysical properties of non-covalently functionalized graphene nanoplatelets nanofluids, Energy Conversion and Manag. 116 (2016) 101–111.

[46] M. Silakhori, H. Fauzi, M.R. Mahmoudian, H.S.C. Metselaar, T.M.I. Mahlia, H. M. Khanlou, Preparation and thermal properties of form-stable phase change materials composed of palmitic acid/polypyrrole/graphene nanoplatelets, Energy Build. 99 (2015) 189–195.

[47] T. Yousefi, F. Veysi, E. Shojaeizadeh, S. Zinadini, An experimental investigation on the effect of Al2O3–H2O nanofluid on the efficiency of flat-plate solar collectors, Renew. Energy 39 (1) (2012) 293–298.

[48] T. Yousefi, E. Shojaeizadeh, F. Veysi, S. Zinadini, An experimental investigation on the effect of pH variation of MWCNT–H2O nanofluid on the efficiency of a flat-plate solar collector, Solar Energy 86 (2) (2012) 771–779.

[49] E. Shojaeizadeh, F. Veysi, Development of a correlation for parameter controlling using exergy efficiency optimization of an Al 2 O 3 /water nanofluid based flat-plate solar collector, Appl. Therm. Eng. 98 (2016) 1116–1129.

[50] Z. Said, M. Sabiha, R. Saidur, A. Hepbasli, N. Rahim, S. Mekhilef, T. Ward, Performance enhancement of a Flat Plate Solar collector using titanium dioxide nanofluid and polyethylene glycol dispersant, J. Clean. Prod. 92 (2015) 343–353.

[51] S.K. Verma, A.K. Tiwari, D.S. Chauhan, Experimental evaluation of flat plate solar collector using nanofluids, Energy Conversion and Manag. 134 (2017) 103–115.

[52] Z. Said, R. Saidur, M. Sabiha, N. Rahim, M. Anisur, Thermophysical properties of single wall carbon nanotubes and its effect on exergy efficiency of a flat plate solar collector, Solar Energy 115 (2015) 757–769.

[53] Y.Y. Gan, H.C. Ong, T.C. Ling, N. Zulkifli, C.-.T. Wang, Y.-.C. Yang, Thermal conductivity optimization and entropy generation analysis of titanium dioxide nanofluid in evacuated tube solar collector, Appl. Therm. Eng. 145 (2018) 155–164.

[54] S. Sami, N. Etesami, Improving thermal characteristics and stability of phase change material containing TiO2 nanoparticles after thermal cycles for energy storage, Appl. Therm. Eng. 124 (2017) 346–352.

[55] C. Ho, J. Gao, Preparation and thermophysical properties of nanoparticle-in-paraffin emulsion as phase change material, Int. Commun. Heat and Mass Transf. 36 (5) (2009) 467–470.

[56] H. Li, L. Wang, Y. He, Y. Hu, J. Zhu, B. Jiang, Experimental investigation of thermal conductivity and viscosity of ethylene glycol based ZnO nanofluids, Appl. Therm. Eng. 88 (2015) 363–368.

[57] D.D.W. Rufuss, S. Iniyan, L. Suganthi, D. Pa, Nanoparticles enhanced phase change material (NPCM) as heat storage in solar still application for productivity enhancement, Energy Procedia 141 (2017) 45–49.

[58] J.L. Zeng, Z. Cao, D.W. Yang, F. Xu, L.X. Sun, X.F. Zhang, L. Zhang, Effects of MWNTS on phase change enthalpy and thermal conductivity of a solid-liquid organic PCM, J. *Therm. Anal. Calorimetry* 95 (2009) 507–512.

[59] S. Zhang, J.-.Y. Wu, C.-.T. Tse, J. Niu, Effective dispersion of multi-wall carbon nano-tubes in hexadecane through physiochemical modification and decrease of supercooling, Solar Energy Mater. Solar Cells 96 (2012) 124–130, https://doi.org/10.1016/j.solmat.2011.09.032.

[60] D. Choi, J. Lee, H. Hong, Y.T. Kang, Thermal conductivity and heat transfer performance enhancement of phase change materials (PCM) containing carbon additives for heat storage application, Int. J. Refrig. 42 (2014), https://doi.org/10.1016/j.ijrefrig.2014.02.004.

[61] Y.A. Çengel, A.J. Ghajar, Heat and Mass Transfer Fundamentals & Applications, McGraw-Hill Education, New York, NY, 2015, pp. 539–544.